Available online at www.sciencedirect.com

SciVerse ScienceDirect

Ceramics International 39 (2013) 1103–1109

CERAMICS INTERNATIONAL

www.elsevier.com/locate/ceramint

Vapor phase synthesis of hexagonal shaped single crystal yttria stabilized zirconia nanoparticles using CO_2 laser

J. Khare[a,*], H. Srivastava[b], C.H.P. Singh[a], M.P. Joshi[a], L.M. Kukreja[a]

[a]*Laser Materials Processing Division, Raja Ramanna Centre for Advanced Technology, Indore-452013, India*
[b]*Indus Synchrotrons Utilization Division, Raja Ramanna Centre for Advanced Technology, Indore-452013, India*

Received 20 March 2012; received in revised form 6 July 2012; accepted 6 July 2012
Available online 20 July 2012

Abstract

Growth of hexagonal shaped single crystal yttria stabilized zirconia nanoparticles has been observed in the vapors emanating from solid targets vaporized using CO_2 laser in CW and pulsed modes of operation. The mean size and yttrium concentration in these nanoparticles are found to be in the range of 5–40 nm and ~10.4–11.6 wt% respectively, which depend on the laser power density and the gaseous environment used during the growth process. Nanoparticles synthesized with pulsed mode of laser operation were found to be smaller in size compared to those generated in the CW mode. It was also found that formation of these nanoparticles was more pronounced in helium gas environment compared to those in nitrogen and argon. X-ray and electron diffraction studies showed that in all experimental conditions the generated nanoparticles were in cubic phase. From high resolution TEM it was observed that the nanoparticles with identical orientations coalesced with each other in line with the oriented attachment theory.

Keywords: Nanoparticles; Zirconia; CO_2 laser; Oriented attachment theory

1. Introduction

Zirconia (ZrO_2) is one of the promising ceramic materials whose nanosized particles are extensively used in various applications such as fuel cell, catalyst, display devices, bio-medical systems etc. Zirconia exists in three phases namely monoclinic, tetragonal and cubic. At room temperature, zirconia is stable in monoclinic phase, and upon heating it transforms to tetragonal and cubic phase at temperature ~1170 °C and ~2360 °C respectively [1]. However, the dopants such as MgO, CaO, CeO, Y_2O_3 etc. can stabilize zirconia in tetragonal and cubic phases at room temperature depending upon their concentrations [1]. Tetragonal and cubic phase zirconia are desirable in several applications such as oxygen sensors [2], catalysts [3], fuel cells [4] etc. For solid oxide fuel cell (SOFC) applications the zirconia based nano powders e.g. yttria-stabilized zirconia (YSZ) are extensively used as electrolyte material because of its high oxygen ion conductivity [5–9]. Therefore efforts are being made for developing simple and cost effective methods for the synthesis of powders of nanometer size YSZ. Several methods such as spray pyrolysis [10], sol–gel based technologies [11], hydrothermal synthesis [12,13], laser ablation [14,15], and laser vaporization (LAVA) [16–19] etc. have been developed for producing YSZ nanoparticles with controlled shape and size. LAVA method has been shown to be effective, economic and versatile technique for large scale production of variety of nanosized particles. Generally it is observed that the zirconia nanoparticles produced by LAVA and laser ablation techniques are mostly of spherical shape [16–19]. Since shape of the nanoparticles also affects the physical and chemical properties, it is therefore important to study the conditions for the growth of nanoparticles of various shapes. The hexagonal YSZ nanoparticles may be particularly interesting for enhancing packaging density of electrolyte in SOFC. In this report we present our studies on CO_2 laser based LAVA method for the growth of hexagonal shaped YSZ nanoparticles in cubic phase. The laser was operated in continuous (CW) and pulsed modes and we investigated the effects of laser

*Corresponding author. Tel.: +91 731 2488383; fax: +91 731 2488380.
E-mail address: jkkhare@rrcat.gov.in (J. Khare).

0272-8842/$ - see front matter © 2012 Elsevier Ltd and Techna Group S.r.l. All rights reserved.
http://dx.doi.org/10.1016/j.ceramint.2012.07.033

power density and ambient gas on the shape, crystalline structure and stoichiometry of the YSZ nanoparticles. The results of these studies are presented and discussed in this paper.

2. Experimental details

A home built transverse flow CO_2 laser was used in the present study with maximum power of 3 kW in CW mode. Pulsed mode operation of laser was achieved by pulsing the input discharge current through a programmable switched mode power supply. It provided control of pulse repetition rate from 1 Hz to 1 kHz with duty cycle from 10% to 90% [20,21]. The target for the experiments was 5 mm thick and 25 mm diameter YSZ pellets prepared by powder metallurgy route. It involved blending of micron-sized ZrO_2 and Y_2O_3 powder (10 mol%), followed by uniaxial pressing to 10 MPa for 3 min. The pellet was sintered in air with following thermal cycle. Initially the temperature of the pellet was increased to 450 °C at 3 °C/min rate and maintained for 3 h. Later the temperature of the pellet was increased to 1600 °C at the same rate and kept for 4 h and then cooled to room temperature at cooling rate of 3 °C/ min.

Schematic of the LAVA process used for nanoparticle generation is shown in Fig. 1. The YSZ target was mounted inside a vacuum chamber on a rotating holder for uniform irradiation of target material. The chamber was first evacuated to a base pressure of 1 mbar using a rotary vacuum pump, followed by pressurizing with suitable carrier gas upto 600 mbar keeping the gas flow rate at ~6 l/min. Experiments were carried out with helium, argon and nitrogen as carrier gases. Laser was focused on to the target using ZnSe lens of focal length of 220 mm to achieve power density in range of 12–24 kW/cm^2 in CW mode. While for the pulsed mode of LAVA process, the laser was operated at 20 Hz repetition rate with 50% duty cycle providing 3 kW/cm^2 average power density. Under these power densities of laser irradiation the target temperature increases to more than its evaporation temperature. Evaporated target materials are then re-condensed into nanometer sized particles under suitable carrier gas environment. Re-condensed nanoparticles were carried away through carrier gas and collected using a foam filter. YSZ nanoparticles collected from foam filter were characterized using X-ray diffraction (XRD), Energy Dispersive Spectroscopy (EDS) and transmission electron microscopy (TEM).

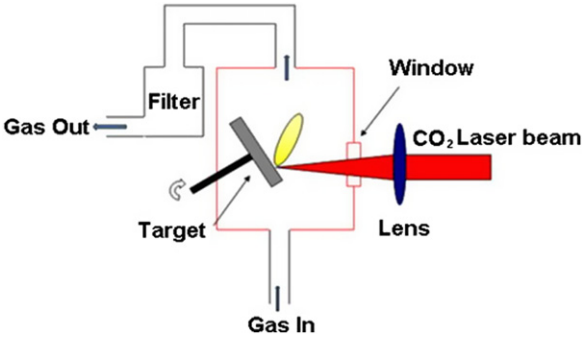

Fig. 1. Schematic of laser vaporization (LAVA) setup.

3. Result and discussion

X-ray diffraction of YSZ nanoparticles obtained with helium, argon, and nitrogen gas environment at different CW and pulsed laser conditions are shown in Fig. 2. All the peaks in the diffraction pattern are similar to fluorite type cubic structure [22]. No peak for yttria, monoclinic or tetragonal zirconia was detected, which indicates that solid solution of yttria and zirconia formed successfully. The most intense peak (111) of the diffraction pattern was used for the estimation of particle size using the Scherrer's formula, $d = 0.89 * \lambda/\beta \cos(\theta)$, where d is crystallite size, λ is wavelength of Cu Kα radiation (1.54 Å), β is peak broadening (in FWHM) and θ is angle of diffraction. Estimated particle sizes are given in Table 1. Under CW mode of laser operation, with different carrier gases, the average particle size is observed to be smallest when helium gas is used. This observation is attributed to higher thermal conductivity of helium gas with respect to argon and nitrogen. Higher thermal conductivity of helium cools the evaporated materials rapidly and therefore restricts the further growth of nanoparticles. When pulsed mode of laser operation is employed with helium as a carrier gas, the average size of the nanoparticles generated were less than those obtained with CW mode of laser operation. This is attributed to less interaction time between plume and laser energy [16]. It is also observed from Table 1 that the estimated size of particles increases as power density increases in CW mode of operation. Power density dependent studies were made only with helium as carrier gas.

Another important feature brought out by X-ray diffraction study is that the (111) diffraction peak for nanoparticles grown using pulsed laser is shifted towards lower 2θ side with respect to those grown using CW laser (see inset in Fig. 2). This preferential reduction in diffraction angle is indicative of increase in inter-planar spacing (d_{111}). This relative increase in inter-planar spacing (or lattice parameter) is possibly due to relative change in the stoichiometry of yttrium in nanoparticles with respect to that in the target material. Energy Dispersive Spectroscopy (EDS) studies were carried out to investigate the possible role of yttrium concentration in YSZ nanoparticles and subsequent increase in the lattice parameter. Table 2 provides chemical composition (in wt%) of YSZ nanoparticles produced with helium environment. It was found that for all laser power densities and in both modes of the laser operation the yttrium concentration in YSZ nanoparticles was lower than the initial yttrium concentration (~13 wt%) in the target material. This observation of loss of yttrium concentration in nanoparticles with respect to target material is commensurate with earlier reports of similar loss of yttrium in powders and thin films produced

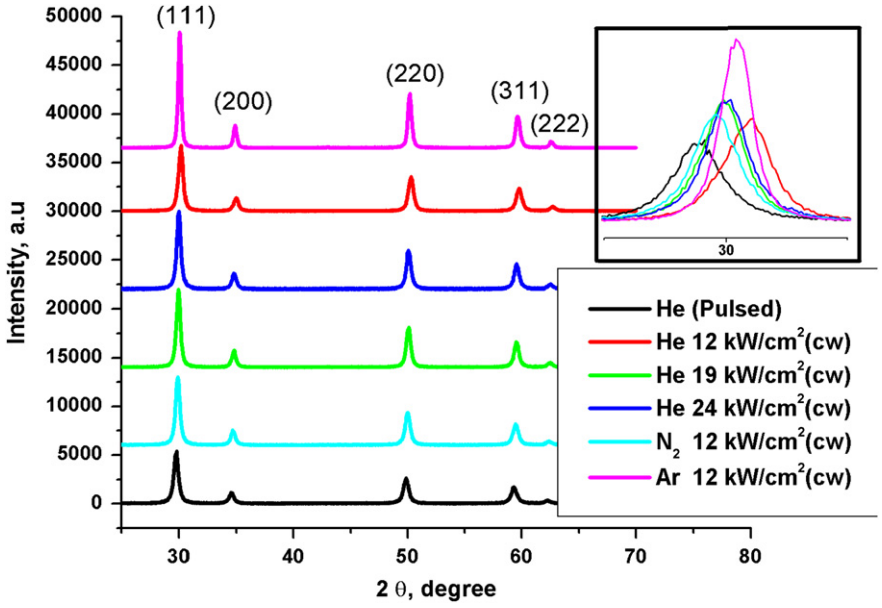

Fig. 2. XRD diffraction patterns of laser generated YSZ nanoparticles under different experimental conditions. Shift in positions of (111) peak is shown as enlarged image in the inset.

Table 1

Power density (kW/cm^2)	Mode of laser operation	Gas	Particle size (nm)	
			XRD	TEM
3 (Average)	Pulsed	He	19.45	9.83
12	CW	He	20.84	17.36
19	CW	He	23.62	15.52
24	CW	He	23.64	12.63
12	CW	N_2	21.80	–
12	CW	Ar	34.61	–

Table 2
YSZ composition of nanoparticles by EDX analysis (wt%).

Power density (kW/cm^2)	Mode of laser operation	Zr	Y	O	Hf
3 (Average)	Pulsed	70.78	11.64	16.93	0.64
12	CW	74.16	10.38	14.66	0.80
19	CW	71.45	11.19	16.41	0.95
24	CW	72.01	11.38	15.8	0.81

by laser evaporation methods [23,24]. However, the relative loss in yttrium concentration in nanoparticles was found to be influenced not only by the mode of laser operation but also the laser power density used. In CW mode of laser operation, the concentration of yttrium in nanoparticles was observed to increase with increase of laser power density. While with the pulsed mode of laser operation the yttrium content in nanoparticles was relatively higher. The possible reasons for the relative increase of yttrium with increase in laser power density could be higher kinetic energy of evaporated materials. Because of higher kinetic energy the evaporated materials follow a straighter path. This leads to reduction in mass-dependent angular spread or scattering and hence generates nanoparticles with composition close to that of the target material [25–27]. While for nanoparticles generated under pulsed mode of laser operation the additional contributing factor for the higher concentration of yttrium (with respect to CW mode of laser operation) could be the shorter interaction time (25 ms, the laser pulse duration). This short interaction time leads to short time for scattering, thereby reducing the relative loss of yttrium. This change in yttrium concentration in laser-generated nanoparticles, as a result of change in mode of laser of operation or associated power density, is responsible for the change in lattice parameter. Kotov et al. reported an increase in lattice parameter of YSZ nanoparticles with increase in its yttria content [23]. Therefore the relatively larger interplanar spacing (d_{111}) or reduced diffraction angle, as observed in Fig. 2, for nanoparticles produced under pulsed mode of laser operation is because of higher yttrium content.

Fig. 3 shows transmission electron micrographs of nanoparticles generated in the pulsed and CW mode of laser operation under helium atmosphere. The particle size distribution histograms of these nanoparticles are shown in Fig. 4. The histogram data were fitted with the Gaussian and log-normal functions. The Gaussian function is given by

$$Y(x) = Y(0) + [A/\{\sigma\sqrt{(\pi/2)}\}] \times \exp[-2 \times (x-\mu)^2/\sigma^2] \quad (1)$$

and the log-normal function is given by

$$Y(x) = Y(0) + [A/(\sigma \times x \times \sqrt{2\pi})]\exp[-\{\ln(x/\mu)\}^2/2\sigma^2] \quad (2)$$

where μ is mean diameter and σ is standard deviation in the respective fitting. The log-normal function provides better fitting in all cases. The mean diameter of nanoparticles

generated in pulsed mode with 3 kW/cm^2 laser power density was ~9.83 nm. While with CW mode of laser operation with power densities 12, 19, and 24 kW/cm^2 the mean diameters of nanoparticles were 17.36, 15.52, and 12.63 nm respectively.

Fig. 5 shows the TEM images of nanoparticles produced in helium, nitrogen and argon atmospheres under CW mode of laser operation with power density of ~12 kW/cm^2. The size distribution histograms of nanoparticles generated in nitrogen and argon atmosphere were also best fitted with the log-normal function. Particles produced with helium gas were observed to be smaller in size and weakly agglomerated while in case of argon and nitrogen as carrier gas the nanoparticles were of large size with substantial agglomeration. This shows that the nature of carrier gas strongly affects the particle formation and growth dynamics. This could be explained on the basis of difference in thermal conductivities of different gases. As the thermal conductivity of the carrier gas decreases ($K_{Ar} < K_{N_2} < K_{He}$) the cooling rate of evaporated material also decreases. This enhances the collision probability of evaporated materials that leads to the growth of large sized aggregated particles.

For detailed information about the internal structure and the morphology of nanoparticles we studied the Selected Area Electron Diffraction (SAED) pattern. Fig. 6 shows the SAED pattern of nanoparticles grown using CW laser with helium carrier gas. The ring type diffraction pattern indicates random orientation of nanocrystals. Similar SAED patterns were obtained for nanoparticles generated in other experimental conditions. Analysis of SAED patterns indicate cubic phase of generated YSZ nanoparticles. First ring corresponds to {111} plane of the cubic phase of zirconia and second, third and fourth rings correspond to {200}, {220} and {311} planes of the cubic phase of zirconia respectively. High resolution TEM (HRTEM) micrograph of nanoparticles, as shown in Fig. 7, suggests most of the particles are hexagonal shaped single crystallites. It also shows that crystal lattice planes are perfectly aligned. The lattice spacing is about ~0.3 nm corresponding to the interplanar spacing of {111} planes.

The comparison of average size of nanoparticles obtained from XRD and TEM image analysis is also shown in Table 1. Analysis of TEM micrographs showed that nanoparticles mean size decreases with increase in laser power density in CW mode of laser operation. While XRD analysis suggests particle size increases with increase in laser power density. This contradictory dependence of particle size with power density can be attributed to the hexagonal shape of particles and the method of sample preparation for XRD and TEM measurement [28,29]. The high resolution TEM (HRTEM) image, as shown in Fig. 7, clearly shows hexagonal shaped morphology of YSZ nanoparticles. As hexagonal shape is best known for high filling factor, therefore during sample preparation for XRD measurement the particles may agglomerate along their edges due to the Van der Waals force and hence reduces the probability of measuring diffraction pattern from an isolated nanoparticle. While in TEM measurement these weakly agglomerated particles are broken into individual particles by sonication and hence can be imaged individually.

The hexagonal shape and single crystalline nature of nanoparticles of YSZ are of particular interest. Most of the reports on synthesis of YSZ nanoparticles grown via LAVA method have shown polycrystalline and spherical shape nanoparticles of YSZ [18,30]. We have obtained single crystalline hexagonal shape nanoparticles of YSZ using LAVA based method which may be of advantage for applications such as electrolyte for oxygen sensor and SOFC. The observation of hexagonal shape nanoparticles

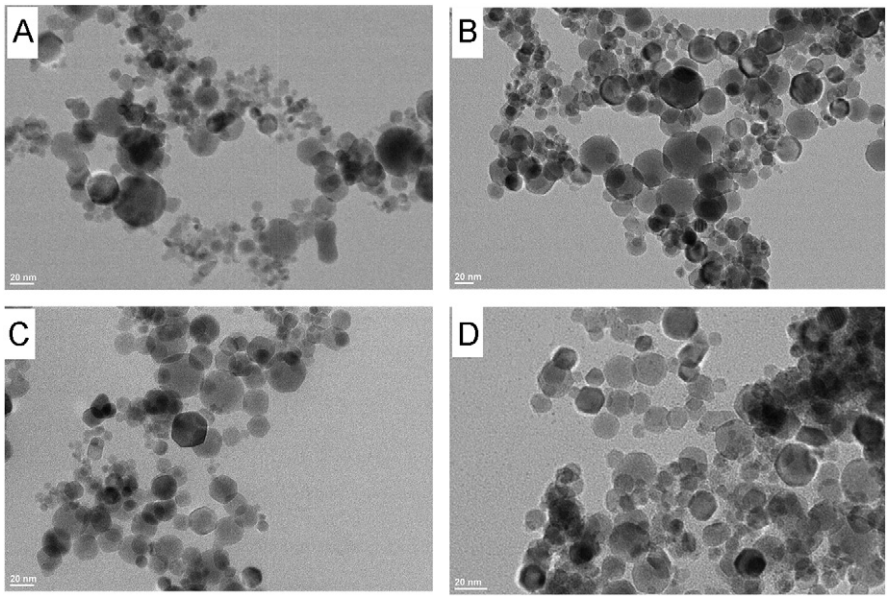

Fig. 3. TEM images of YSZ nanoparticles produced under helium gas atmosphere grown under (A) pulsed mode of laser operation with power density of 3 kW/cm^2 and under CW mode of laser operation with power density (B) 12 kW/cm^2, (C) 19 kW/cm^2 and (D) 24 kW/cm^2.

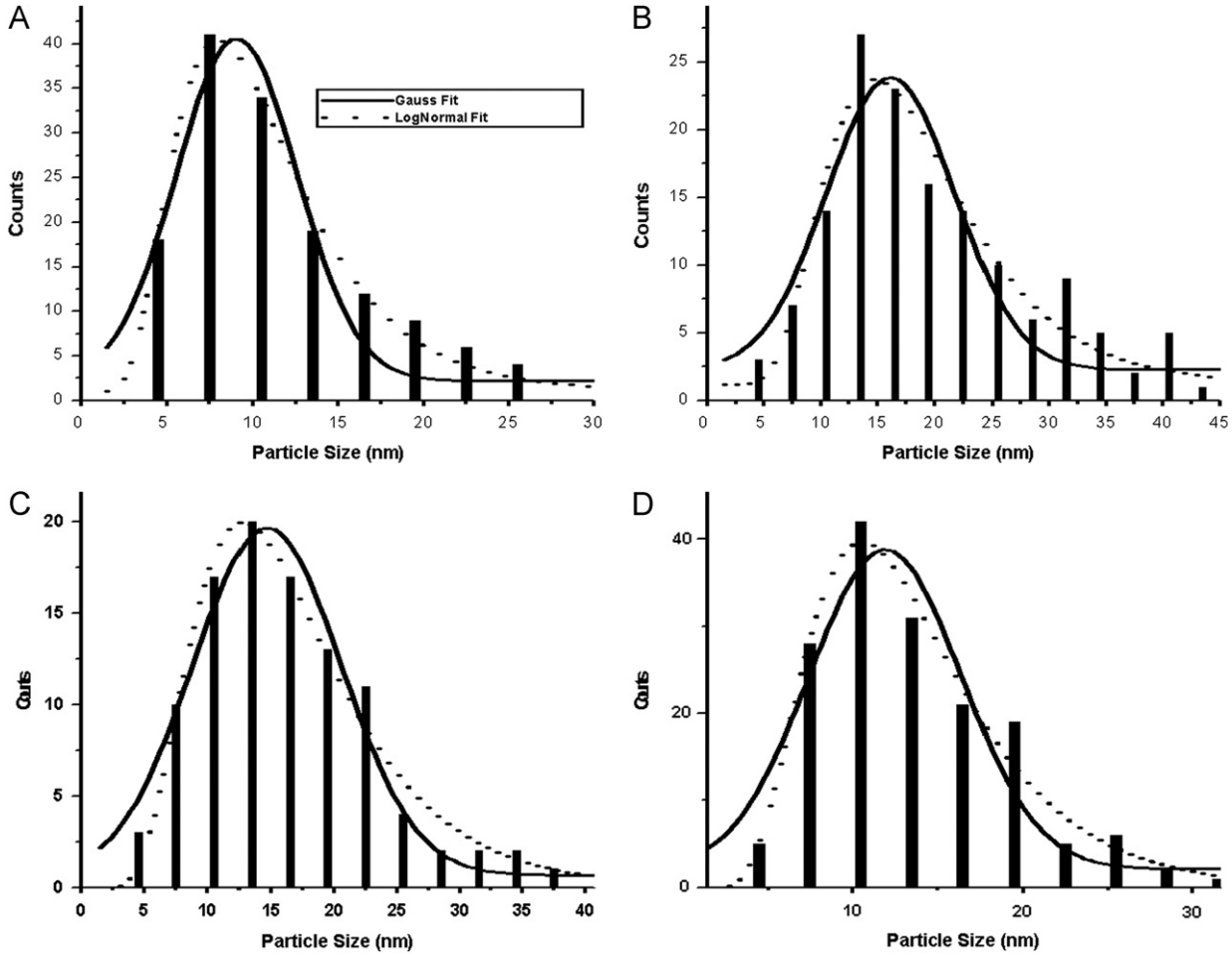

Fig. 4. Histograms of size distribution of YSZ nanoparticles shown in Fig. 3.

of YSZ in our experimental setup could be due to different conditions of evaporation process and re-condensation parameters. Two different models are widely used to explain the growth and final morphology of particles following the bottom up approach of growth. The first one is the classical crystal growth theory or Oswald ripening (OR) theory [31] and other is Oriented Attachment (OA) theory [32]. According to the OR theory the larger particles grow by consumption of smaller particles because the total surface energy of small particles is high compared to surface energy of large particles. In the OA theory, particles grow into single crystal or twins through self-organization by sharing a common crystallographic orientation. This self-organization growth mode plays very important role in producing peculiar morphology of nanoparticles. OA theory has been successfully used to explain the growth process of different shape of nanoparticles synthesized by the hydrothermal, vapor phase and wet chemical methods [32,33]. We consider the OA theory for explaining the formation of hexagonal shape nanoparticles of YSZ.

Synthesis of nanoparticles by the LAVA method involves two processes namely the nucleation and the growth. Final morphology of nanoparticles is affected by both these processes. Under OA mechanism two or more particles organized themselves in such a way that they share a common crystallographic orientation and form a single crystal or twins. HRTEM image of particles coagulated along a common crystallographic axis, as shown in Fig. 8, further confirms and compliments the growth of nanoparticles which indeed occurs by OA mechanism. The {111} planes in cubic zirconia is highly stable in comparison with others planes. Therefore to minimize surface energy the primary particles combine in $\langle 1\text{–}10 \rangle$ direction (perpendicular to {111} plane) and $\langle 111 \rangle$ direction (parallel to {111} plane) by sharing a common crystallographic orientation and grow in hexagonal shape because the Van der Waals forces are minimum at hexagonal faces [33].

4. Conclusion

Laser vaporization based method was used for the generation of yttria-stabilized zirconia (YSZ) nanoparticles. Under the conditions of the experimental parameters we observed hexagonal shaped YSZ nanoparticles in cubic phase. Comparative studies were carried out for the synthesis of these nanoparticles under three different gas environments namely helium, nitrogen, and argon and in

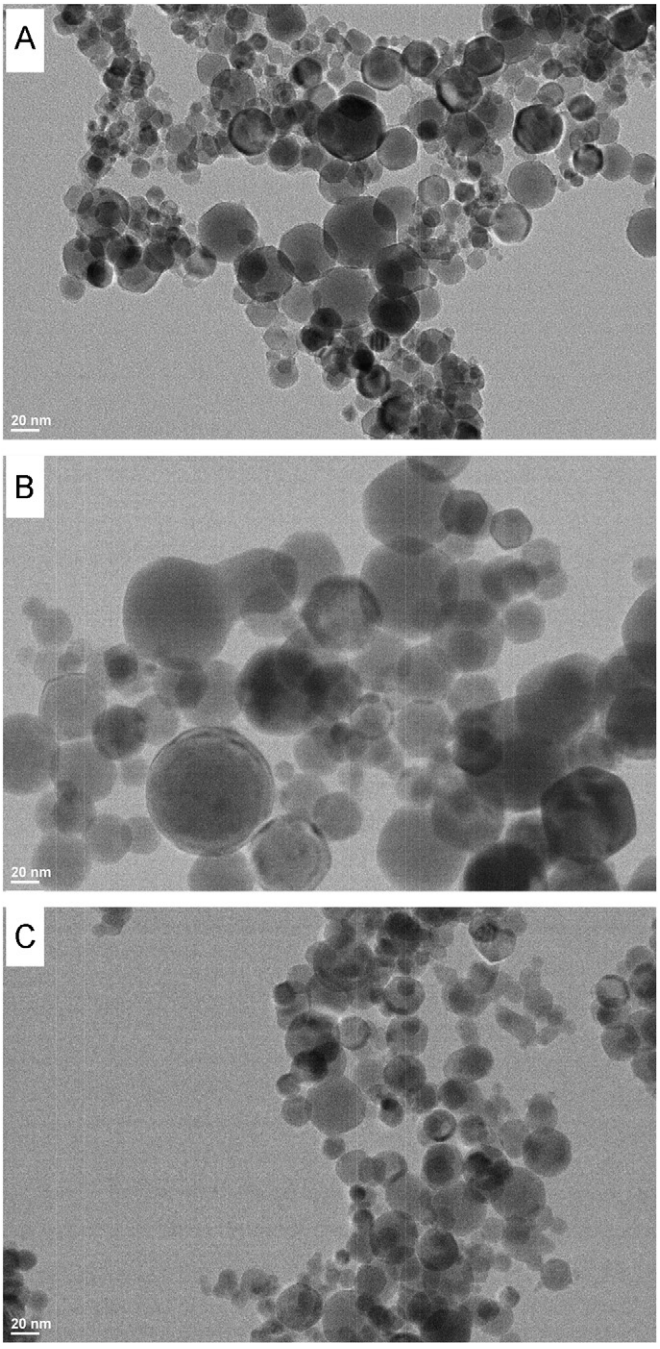

Fig. 5. TEM images of YSZ nanoparticles produced at power density 12 kW/cm^2 in (A) helium, (B) nitrogen and (C) argon gases.

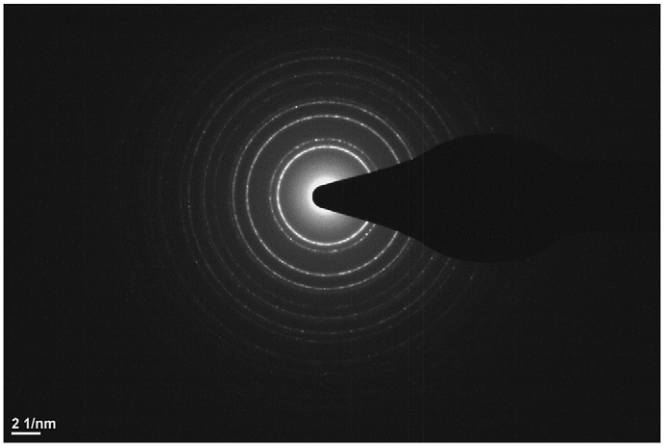

Fig. 6. Selected Area Electron Diffraction (SAED) pattern of YSZ nanoparticles produced using CW laser and under helium gas environment.

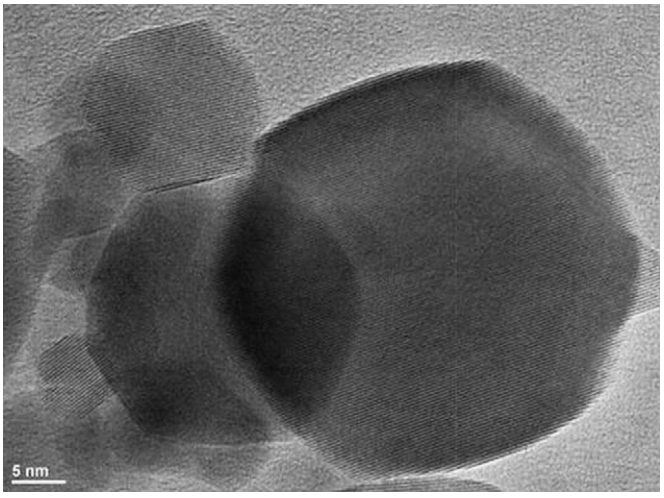

Fig. 7. HRTEM images of YSZ nanoparticles produced using CW laser and under argon atmosphere.

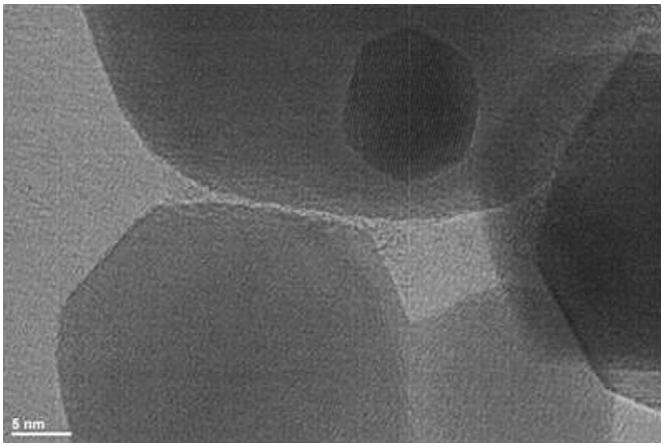

Fig. 8. Common crystallographic orientation of YSZ nanoparticles produced using CW laser under helium atmosphere.

two modes of laser operation i.e. pulsed and CW. Formation of hexagonal shaped YSZ nanoparticles was more pronounced in helium gas environment compared to nitrogen and argon. The mean size and yttrium concentration in these nanoparticles were found to depend on the laser power density and the environment during the growth process. The mean size of nanoparticles was smallest and nanoparticles were less agglomerated in pulsed mode of laser operation compared to those nanoparticles generated in the CW mode of laser operation. X-ray and electron diffraction studies showed that in all experimental conditions the generated nanoparticles were in cubic phase. Possible mechanism of hexagonal shape of nanoparticles was provided on the basis of the OA theory.

Acknowledgments

The authors acknowledge Mr. Anil R. Adbol and Mr. Prabhu U. Sangale for their help in performing the experiment. We also acknowledge Shri Rakesh Kaul for suggestions and critical reading of the manuscript.

References

[1] R.H.J. Hannink, Zirconia–The Cinderella transformation, Materials Forum 23 (1999) 153–177.
[2] O.K. Tan, W. Cao, Y. Hu, W. Zhu, Nano-structured oxide semiconductor materials for gas-sensing applications, Ceramics International 30 (2004) 1127–1133.
[3] X. Qi, M. Watanabe, T.M. Aida, R.L. Smith Jr., Sulfated zirconia as a solid acid catalyst for the dehydration of fructose to 5-hydroxymethylfurfural, Catalysis Communications 10 (2009) 1771–1775.
[4] Y. Zhang, J. Gao, D. Peng, M. Guangyao, X. Liu, Dip-coating thin yttria-stabilized zirconia films for solid oxide fuel cell applications, Ceramics International 30 (2004) 1049–1053.
[5] T.J. Pennycook, M.P. Oxley, J.G. Barriocanal, F.Y. Bruno, C. Leon, J. Santamaria, S.T. Pantelides, M. Varela, S.J. Pennycook, Seeing oxygen disorder in YSZ/$SrTiO_3$ colossal ionic conductor hetero structures using EELS, European Physical Journal of Applied Physics 54 (2011) 33507.
[6] X. Guo, Can we achieve significantly higher ionic conductivity in nanostructured zirconia, Scripta Materialia 65 (2011) 96–101.
[7] Y.J. Leng, S.H. Chan, K.A. Khor, S.P. Jiang, Performance evaluation of anode-supported solid oxide fuel cells with thin film YSZ electrolyte, International Journal of Hydrogen Energy 29 (2004) 1025–1033.
[8] Y. Zhang, J. Gao, D. Peng, M. Guangyao, X. Liu, Dip-coating thin yttria-stabilized zirconia films for solid oxide fuel cell applications, Ceramics International 30 (2004) 1049–1053.
[9] X. Xu, C. Xia, S. Huang, D. Peng, YSZ thin films deposited by spin-coating for IT-SOFCs, Ceramics International 31 (2005) 1061–1064.
[10] W. Widiyastuti, R. Balgis, F. Iskandar, K. Okuyama, Nanoparticle formation in spray pyrolysis under low-pressure conditions, Chemical Engineering Science 65 (2010) 1846–1854.
[11] V.G.D. Arellano, M.I.E. Cabrera, J.R. Gasga, M.E.C. Garcia, Structural study of zirconia nanoclusters by high-resolution transmission electron microscopy, Materials Characterization 52 (2004) 179–186.
[12] M. Gaudon, E. Djurado, N.H. Menzler, Morphology and sintering behaviour of yttria stabilised zirconia (8-YSZ) powders synthesised by spray pyrolysis, Ceramics International 30 (2004) 2295–2303.
[13] L. Kumari, G.H. Du, W.Z. Li, R.S. Vennila, S.K. Saxena, D.Z. Wang, Synthesis microstructure and optical characterization of zirconium oxide nanostructures, Ceramics International 35 (2009) 2401–2408.
[14] M.H. Tsai, S.Y. Chen, R. Shen, P. Shen, Laser ablation condensation of polymorphic ZrO_2 nanoparticles: effects of laser parameters, residual stress, and kinetic phase change, Journal of Applied Physics 99 (2006) 054302.
[15] G.F. Gaertner, H. Lydtin, Reviw of ultrafine particle generation by laser ablation from solid targets in gas flows, NanoStructured Materials 4 (1994) 559–568.
[16] G. Staupendahl, G. Michel, G. Eberhardt, E. Mu¨ller, Ch. Oestreich, W. Vogelsberger, J. Schlegel, Production of nanosized zirconia particles by pulsed CO_2 laser evaporation, Journal of Laser Applications 11 (1999) 14–20.
[17] M.G. Ivanov, Yu.A. Kotov, A.I. Medvedev, A.M. Murzakayev, V.V. Osipov, A.K. Shtolz, V.I. Solomonov, Metastable states of laser synthesized oxide nanoparticles, Journal of Alloys and Compounds 483 (2009) 503–506.
[18] U. Lohbauer, A. Wagner, R. Belli, C. Stoetzel, A. Hilpert, H.D. Kurland, J. Grabow, F.A. Müller, Zirconia nanoparticles prepared by laser vaporization as fillers for dental adhesives, Acta Biomaterialia 6 (2010) 4539–4546.
[19] H.D. Kurland, J. Grabow, F.A. Müller, Preparation of ceramic nanospheres by CO_2 laser vaporization (LAVA), Journal of the European Ceramic Society 31 (2011) 2559–2568.
[20] J. Khare, R. Sreedhar, C.P. Paul, T. Reghu, A.K. Nath, Optical characteristics and power scaling of a transverse flow transversely excited CW CO_2 laser, Pramana 60 (2003) 99–107.
[21] B.T. Rao, M.O. Ittoop, L.M. Kukreja, A power ramped pulsed mode laser piercing technique for improved CO_2 laser profile cutting, Optics and Lasers in Engineering 47 (2009) 1108–1116.
[22] E.C. Dickey, X. Fan, Structure and chemistry of yttria-stabilized cubic-zirconia symmetric tilt grain boundaries, Journal of the American Ceramic Society 84 (2001) 1361–1368.
[23] Yu.A. Kotov, V.V. Osipov, M.G. Ivanov, O.M. Samatov, V.V. Platonov, V.V. Lisenkov, A.M. Murzakayev, A.I. Medvedev, A.K. Shtolz, O.R. Timoshenkova, Properties of YSZ and CeGdO nanopowders prepared by target evaporation with a pulse-repetitive CO_2 laser, Reviews on Advanced Materials Sciience 5 (2003) 171–177.
[24] E. Vasco, L. VaHzquez, M. AguiloH, C. Zaldo, Epitaxial growth of Y-stabilised zirconia films on (1 0 0) InP substrates by pulsed laser deposition, Journal of Crystal Growth 209 (2000) 883–889.
[25] S. Acquaviva, E. D'Anna, M.L. De Giorgi, M. Fernandez, A. Luches, G. Majni, S. Luby, E. Majkova, Transfer of stoichiometry during pulsed laser ablation of multicomponent magnetic targets, Applied Surface Science 248 (2005) 286–290.
[26] H. Dang, Q. Qin, Angular distribution of laser-ablated species from a $Pr_{0.67}Sr_{0.33}MnO_3$ target, Physical Review B 60 (1999) 1187–1192.
[27] C.B. Arnold, M.J. Aziz, Stoichiometry issues in pulsed-laser deposition of alloys grown from multicomponent targets, Applied Physics A 69 (1999) S23–S27.
[28] Y. Zhong, D. Ping, X. Song, F. Yin, Determination of grain size by XRD profile analysis and TEM counting in nano-structured Cu, Journal of Alloys and Compounds 476 (2009) 113–117.
[29] H. Zhanga, D.D. Wang, Denga Li-Er, Z.T. An, Q. Tang, Y.S. Wang, W.C. Li, Comparative study of calculated and TEM characterization sizes of peanut-like nano-grains in mesoporous c-ZrO_2 microspheres, Materials Characterization 59 (2008) 493–497.
[30] H. Ferkel, J. Naser, W. Riehemann, Laser induced solid solution of the binary nanoparticles system, Nanostructured Materials 8 (1997) 457–464.
[31] X. Ren, D. Han, D. Chen, F. Tang, Large-scale synthesis of hexagonal cone-shaped ZnO nanoparticles with a simple route and their application to photocatalytic degradation, Materials Research Bulletin 42 (2007) 807–813.
[32] J. Zhang, F. Huang, Z. Lin, Progress of nanocrystalline growth kinetics based on oriented attachment, Nanoscale 2 (2010) 18–34.
[33] K.Y. Chick, M. Nath, B.A. Parkinson, TaS_2 nanoplatelets, produced by laser ablation, Journal of Materials Research 21 (2006) 1243–1247.